Correcting Optical-Axis Calculation in Polarization-Sensitive Optical Coherence Tomography

Chuanmao Fan and Gang Yao*, *Member, IEEE*

***Abstract*—Polarization-sensitive optical coherence tomography (PSOCT) has found many applications in imaging birefringence tissue samples. Polarization-sensitive detection is often implemented by utilizing a circularly polarized incident light and detecting the two orthogonal horizontal- and vertical-polarized interference components. However, the obtained optical axes images were inappropriately represented as depth-dependent periodic maps in all reported studies. A detailed analysis confirmed that this misrepresentation was caused by the accumulation of optical retardation with depth. A simple method was proposed to numerically correct this optical-axis calculation. Experimental studies in tendon tissue demonstrated that this method can be applied to map the 2-D optical-axis distributions in enface PSOCT images.**

***Index Terms*—Biomedical optical imaging, image processing, optical imaging, polarization.**

I. Introduction

POLARIZATION-SENSITIVE optical coherence tomography [1]–[3] (PSOCT) is an important branch of optical coherence tomography (OCT). It can provide extra polarization contrast mechanisms, including retardation and optical-axis orientation in addition to structural information. Many technologies have been developed, such as Stokes vectors imaging [4], Jones matrix [5], [6], and Muller matrix measurements [7], [8]. Among various implementations, the approach reported by Hitzenberger *et al.* [3] is the simplest that used a circularly polarized incident light and detected the horizontal- and vertical-polarized components. This method has been implemented in both bulk [9] and fiber-based [10] frequency-domain PSOCT. Due to its simplicity, it has also been adopted by several different single-detector PSOCT implementations [11]–[18]. This algorithm has been widely used to image the retardation and optical-axis orientation in a variety of birefringence tissues, such as skin [16], nail bed [17], [18], retina [9], [10], [23], cornea [21], muscle [12], [15], tendon [12]–[15], atherosclerotic plaques [19], and other birefringence materials [20], [22]. However, in all these studies, the optical-axis maps appeared as a periodic structure varying between $-\pi$ and $+\pi$ that does not represent the true optical axis in the sample. Since optical axis is essential for identifying fiber orientations, its misrepresentation hinders a direct visualization of fiber orientations in birefringence samples.

In this letter, we analyzed the computational mechanism in PSOCT and confirmed that such axis misrepresentation was caused by the retardation accumulation at different sample depths [3]. A simple method was then proposed to correct this effect. Experimental verification was conducted to demonstrate this method in birefringence tissue samples.

II. Method

A. Cause of Incorrect Optical-Axis Calculation

In PSOCT, the optical component and tissue sample can be described by using the Jones matrix [5], [6] method. In a typical PSOCT system [9], [10], a circularly polarized incident light was produced in the sample arm after passing a vertically polarized light through a quarter wave plate. The round-trip polarization state of the reflectance light from the sample can be calculated by using Jones matrix multiplication [9], [10]

$$\begin{pmatrix} E_H^s \\ E_V^s \end{pmatrix} = \mathbf{J}_Q \mathbf{J}_S^T \mathbf{J}_S \mathbf{J}_Q \mathbf{E}_{\text{in}} = \frac{1}{2}\begin{pmatrix} 1 & i \\ i & 1 \end{pmatrix} \mathbf{J}_S^T \sqrt{R} \mathbf{J}_S \begin{pmatrix} 1 & i \\ i & 1 \end{pmatrix} \begin{pmatrix} 0 \\ 1 \end{pmatrix} E_0 \quad (1)$$

where R is the reflectivity of the sample, $\mathbf{J}_Q$ is the Jones matrix of a quarter wave plate, and $\mathbf{J}_S$ represents the Jones matrix of a birefringence sample as follows (2), as shown at the bottom of the next page, where δ is the retardation (phase difference between E_H and E_V induced by the sample), and θ is the fast optical axis (perpendicular to fiber orientation). As delineated previously [3], the measured depth-resolved H- and V-polarized component (A_H and A_V) of the image signal after applying Fourier transform to the interference spectrum are as follows:

$$\begin{bmatrix} A_H(z) \\ A_V(z) \end{bmatrix} = \begin{bmatrix} E_r E_s(z) \cos(\delta) \exp\left[i\left(2kz + \frac{\pi}{2} + \varphi_{\text{rand}}\right)\right] \\ E_r E_s(z) \sin(\delta) \exp\left[i\left(2kz + \frac{3\pi}{2} - 2\theta + \varphi_{\text{rand}}\right)\right] \end{bmatrix} \quad (3)$$

where E_r and E_s are amplitudes of the reference and sample light, respectively, for both H- and V-polarized component. φ_{rand} is the common random phase, and $2kz$ is the round-trip phase difference between the reference and sample arms. The sample retardation can be calculated as $\delta = \tan^{-1}(|A_V|/|A_H|)$.

Manuscript received March 29, 2010; revised May 31, 2010; accepted June 17, 2010. Date of publication June 28, 2010; date of current version September 15, 2010. This work was supported in part by the National Science Foundation under Grant CBET06431990. *Asterisk indicates corresponding author.*

C. Fan is with the Department of Biological Engineering, University of Missouri, Columbia, MO 65211 USA (e-mail: cf7b6@mail.missouri.edu).

*G. Yao is with the Department of Biological Engineering, University of Missouri, Columbia, MO 65211 USA (e-mail: yaog@missouri.edu).

Digital Object Identifier 10.1109/TBME.2010.2053927

To calculate the corresponding optical axis, the product of A_V and the conjugate of A_H was calculated as follows:

$$A = A_V A_H^* = E_r^2 E_s^2(z)\sin(\delta)\cos(\delta)\exp[i\phi] \quad (4)$$

where $\phi = \pi - 2\theta$. The orientation of optical axis θ ranges from 0 to π and is calculated from the phase angle of A as follows:

$$\theta = \frac{\pi}{2} - \frac{1}{2}\text{angle}[A]. \quad (5)$$

The calculated phase angle, i.e., angle[A], has a range of $[-\pi, \pi]$ and is affected by the sign of the retardation term $\sin(\delta)\cos(\delta)$. As an example, for $0 \le \phi \le \pi/2$, if the retardation is located in the first or third quadrant, a correct θ is calculated. But if δ is in the second or fourth quadrant, then the angle[A] is interpreted as an angle in the third quadrant because of the negative sign of $\sin(\delta)\cos(\delta)$, thus resulting in a $+\pi/2$ phase wrapping to the calculated θ. Similarly, for $\pi \le \phi \le 3\pi/2$, a correct θ is obtained from (5), if δ is in the first or second quadrant. However, angle[A] is interpreted as an angle in the first quadrant, if δ is in the second or fourth quadrant, resulting in an apparent $-\pi/2$ phase addition to the calculated θ. In PSOCT, the accumulation of retardation δ with sample thickness thus produces an apparent periodic change of the optical axis with imaging depth.

B. Correcting Retardation Effect

Such retardation-accumulation-induced change in optical axis could theoretically be corrected by identifying the transition point of the retardation or optical axis and correcting any sudden changes. However, OCT images in tissue are known to be prone to speckle noise, which makes it challenging in identifying true transitional points. Therefore, a method that can automatically correct this problem would have significant practical advantages.

In our method, a π phase term was digitally added to the vertically polarized component of the detected signal A_V

$$A_V' = E_r E_s(r)\sin(\delta)\exp\left[i\left(2kz + \frac{3\pi}{2} - 2\theta + \varphi_{\text{rand}}\right)\right] \times \exp(i\pi). \quad (6)$$

The effect of this phase term is equivalent to a multiplication with -1. The product of A_V' and A_H^* was then calculated as

$$A' = A_V' A_H^* = E_r^2 E_s^2(z)\sin(\delta)\cos(\delta)\exp[i\phi'] \quad (7)$$

where $\phi' = -2\theta$ and has a range of $[-\pi, \pi]$. The resulting optical-axis orientation can be calculated as follows:

$$\theta' = -\frac{1}{2}\text{angle}[A']. \quad (8)$$

If the top tissue layer has a negative θ', a constant of π is added to maintain a range of [0, π] for the θ'. Because of the π phase induced, the retardation-induced phase change in angle[A'] was reversed as that in angle[A]. Thus, its effect was eliminated when adding the two together. The true optical axis can then be obtained as follows:

$$\theta = \frac{\pi}{4} - \frac{1}{4}(\text{angle}[A] + \text{angle}[A']). \quad (9)$$

C. Experimental Demonstration

Experiments were conducted to demonstrate the proposed algorithm using a PSOCT system. A detailed description of the system has been reported elsewhere [24]. It was a spectral-domain full-range PSOCT. One SLD at 844 nm ($\Delta\lambda_0 =$ 46.8 nm) was used as the light source.The axial and lateral resolutions were 6.7 and 32 μm, respectively. The system speed was 50 000 A-lines/s.The A-B-C scan size was 1024 $\times$ 1000 $\times$ 500 pixels corresponding to a scan range of 5.2 mm $\times$ 4.9 mm $\times$ 4.9 mm. Intensity, phase retardation, and optical-axis orientation images were obtained, as described in Section II-A and II-B.

III. Results and Discussion

A. Simulation

Numerical simulation was first conducted to demonstrate the retardation effect and the correction algorithm introduced in Section II. In the simulation, a stack of N layers of wave plates was used to simulate a birefringence sample. Each wave plate was modeled by a Jones matrix $\mathbf{J}_i$ and the round-trip Jones matrix of the N-layer wave-plates stack represented the polarization-sensitive measurement of the Nth layer in a conventional PSOCT

$$\mathbf{J}(N) = \mathbf{J}_1^T \ldots \mathbf{J}_{N-1}^T \mathbf{J}_N^T \mathbf{J}_N \mathbf{J}_{N-1} \ldots \mathbf{J}_1. \quad (10)$$

Each individual wave plate had a fixed identical birefringence $\Delta n = 5 \times 10^{-4}$. The optical axis of each wave plate in the stack varied randomly at $[-2.5^\circ, 2.5^\circ]$ around a central-axis orientation of 62.5°.

Both the conventional method and our proposed correction algorithm were applied to calculate the optical axis and retardation with a circularly polarized incident light. As shown in Fig. 1, the conventional (uncorrected) axis measurement had a π phase jump when the accumulative retardation increased to 45° (single trip) and again to 135°. In other words, it led to a 90° phase change in the measured optical axis for every 90° increment in double-trip retardation. However, the proposed algorithm successfully eliminated the retardation effect and fully recovered the theoretical axis.

$$\mathbf{J}_S = \begin{bmatrix} \cos\left(\frac{\delta}{2}\right) + i\sin\left(\frac{\delta}{2}\right)\cos(2\theta) & i\sin\left(\frac{\delta}{2}\right)\sin(2\theta) \\ i\sin\left(\frac{\delta}{2}\right)\sin(2\theta) & \cos\left(\frac{\delta}{2}\right) - i\sin\left(\frac{\delta}{2}\right)\cos(2\theta) \end{bmatrix} \quad (2)$$

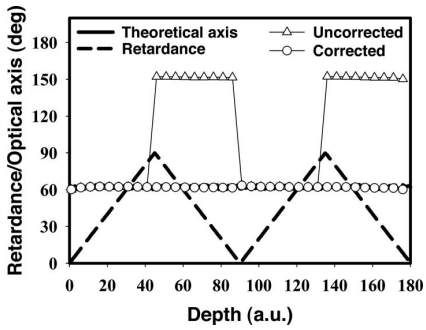

Fig. 1. Simulated PSOCT measurements in a stack of wave plates.

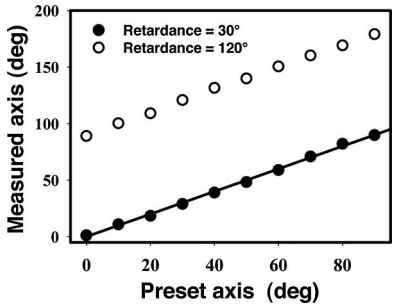

Fig. 2. Optical axis measured with retardation in the first quadrant (30°) and second quadrant (120°). Axis measured with retardation in the second quadrant experienced a 90° phase change. The solid line represents the preset values.

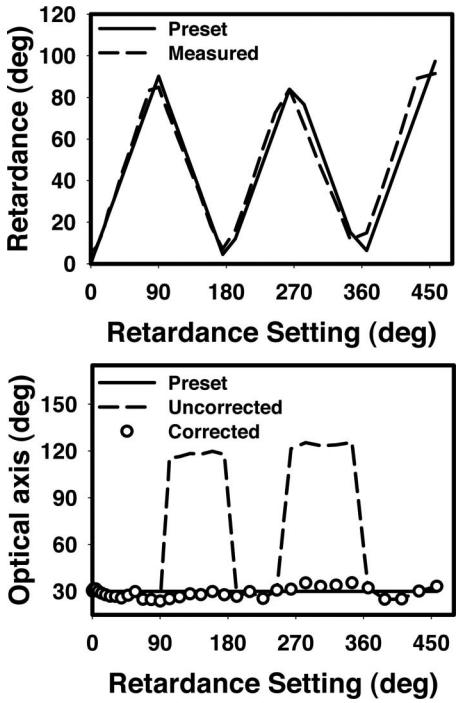

Fig. 3. Optical axis and retardation measurements of a variable wave plate at different retardation settings. The optical axis was set at 30° during the measurements. The theoretical, uncorrected, and corrected measurement results were shown.

B. Tests in Wave Plate

To illustrate the retardation-induced phase-shifting phenomenon in optical-axis measurement, the optical axis of a Berek compensator (5540, New Focus, Santa Clara, CA) was measured using our PSOCT system. The optical axis was measured when the retardation was set in the first quadrant [0, π/2] and the second quadrant [π/2, π].

As shown in Fig. 2, when the retardance was set in the first quadrant (30°), the measured optical axis had an excellent agreement with the preset values. However, the axis measurement with the retardance in the second quadrant (120°) had a 90° jump as expected. When the correction algorithm was used, the 90° addition was removed and the true optical axis was recovered.

Fig. 3 shows the measurement results when the optical axis of the Berek compensator was fixed at 30°, but its retardance was changed gradually. A 90° phase shift in optical axis occurred at retardation of 90°, 180°, 270°, and 360°, which represented the transition points between two consecutive quadrants. The correction algorithm successfully eliminated such sudden phase changes. The retardation measurements had a good agreement with the wave plate settings. The corrected optical axis closely fluctuated around the preset values axis. Part of these errors was due to the movement of the optical mount when adjusting the retardation.

C. Tests in Tendon Samples

A piece of chicken tendon tissue was imaged to further test the proposed algorithm. An enface PSOCT image acquired at $\sim$130 μm below the sample surface is shown in Fig. 4.

The intensity image shows the structural information of the tendon similar to those reported in other studies [12]–[15]. The accumulative retardation and the conventional axis orientation had similar topological periodic patterns. Such periodic patterns did not correctly represent the true optical-axis distribution. In the corrected optical-axis image [see Fig. 4(d)], the periodic patterns were removed leaving a relatively uniform map of optical axis. Fig. 4(e) shows a detailed comparison between uncorrected and corrected optical axis along one B-scan line. As shown in Fig. 4(e), the optical-axis orientation changed graduaLy from $\sim$90° to $\sim$110° when moving from the left boundary to the right boundary. Because the optical axis is perpendicular to the collagen fiber orientation, the collagen fiber orientation can be calculated based on the corrected optical-axis image in Fig. 4(d), as illustrated in Fig. 4(f) using a streamline plot. The morphological changes of fiber orientation appeard to agree with surface texture features shown in the intensity image [see Fig. 4(a)].

As previously recognized [4], the conventional PSOCT implementation [see (1)–(3)] using a single circularly polarized light can only retrieve correct polarization parameters in samples where the optical axis is consistent with depth. This condition is usually satisfied in certain biological tissues, such as tendon especially at small depths. Fig. 5 shows the cross-sectional PSOCT image of the same tendon sample used in Fig. 4. As in the enface image, the retardation-induced periodic changes in optical axis at different depths, as shown in Fig. 5(c), were largely eliminated in the corrected optical-axis image [see Fig. 5(d)]. There are variations in the optical axis across the sample, but the optical axis was relatively stable at small depths.

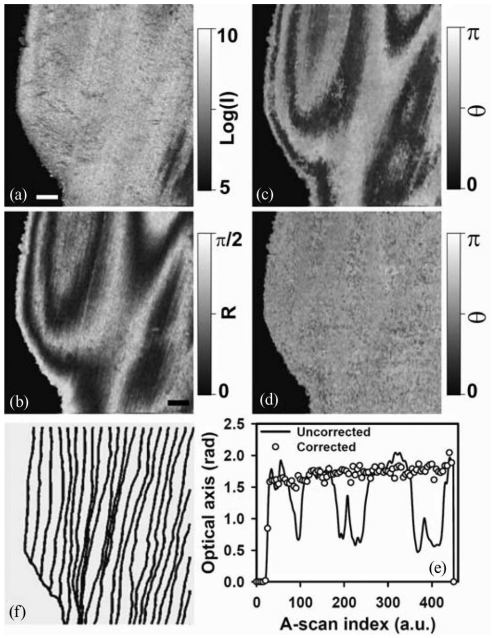

Fig. 4. Enface PSOCT images of a tendon sample. (a) Intensity. (b) Retardation. (c) Conventional uncorrected optical axis. (d) Corrected optical axis mapping. (e) Comparison between uncorrected and corrected optical axis along one B-scan line across the sample. (f) Streamlines map of fiber orientation. The size bar in the intensity image indicates 0.5 mm.

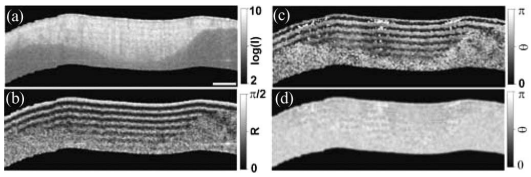

Fig. 5. B-scan PSOCT images of the tendon sample. (a) Intensity. (b) Retardation. (c) Conventional uncorrected optical axis. (d) Corrected optical axis. The size bar in the intensity image indicates a size of 0.5 mm.

IV. Conclusion

We analyzed the retardation-induced misrepresentation of optical axis in a classic implementation of PSOCT. A novel method was proposed to automatically correct the optical-axis calculation using an additional digital phase shift during image reconstruction. This signal-processing method reversed the changes in optical axis induced by the retardation accumulation. Adding this new signal with the original optical-axis calculation thus eliminated any retardation-induced effect. This method can be theoretically applied in any such PSOCT implementations, but it can be conveniently incorporated especially in the frequency-domain PSOCT.We have experimentally shown that this method is capable of revealing the 2-D collagen fiber orientation in enface PSOCT images acquired in a tendon sample.

References

[1] M. R. Hee, D. Huang, E. A. Swanson, and J. G. Fujimoto, "Polarization-sensitive low coherence reflectometer for birefringence characterization and ranging," *J. Opt. Soc. Amer. B*, vol. 9, pp. 903–908, 1992.

[2] J. F. de Boer, T. E. Milner, M. J. C. Van Gemert, and J. S. Nelson, "Two-dimensional birefringence imaging in biological tissue by polarization-sensitive optical coherence tomography," *Opt. Lett.*, vol. 22, pp. 934–936, 1997.

[3] C. K. Hitzenberger, E. Götzinger, M. Sticker, M. Pircher, and A. F. Fercher, "Measurement and imaging of birefringence and optic axis orientation by phase resolved polarization sensitive optical coherence tomography," *Opt. Exp.*, vol. 9, pp. 780–790, 2001.

[4] J. F. de Boer and T. E. Milner, "Review of polarization sensitive optical coherence tomography and stokes vector determination," *J. Biomed. Opt.*, vol. 7, pp. 359–371, 2002.

[5] S. L. Jiao and L. H. V. Wang, "Jones-matrix imaging of biological tissues with quadruple-channel optical coherence tomography," *J. Biomed. Opt.*, vol. 7, pp. 350–358, 2002.

[6] B. H. Park, M. C. Pierce, B. Cense, and J. F. de Boer, "Jones matrix analysis for a polarization-sensitive optical coherence tomography system using fiber-optic components," *Opt. Lett.*, vol. 29, pp. 2512–2514, 2004.

[7] G. Yao and L. V. Wang, "Two-dimensional depth-resolved Mueller matrix characterization of biological tissue by optical coherence tomography," *Opt. Lett.*, vol. 24, pp. 537–539, 1999.

[8] Y. Yasuno, S. Makita, T. Endo, M. Itoh, T. Yatagai, M. Takahashi, C. Katada, and M. Mutoh, "Polarization-sensitive complex fourier domain optical coherence tomography for Jones matrix imaging of biological samples," *Appl. Phys. Lett.*, vol. 85, pp. 3023–3025, 2004.

[9] E. Götzinger, M. Pircher, and C. K. Hitzenberger, "High speed spectral domain polarization sensitive optical coherence tomography of the human retina," *Opt. Exp.*, vol. 13, pp. 10217–10229, 2005.

[10] E. Götzinger, B. Baumann, M. Pircher, and C. K. Hitzenberger, "Polarization maintaining fiber based ultra-high resolution spectral domain polarization sensitive optical coherence tomography," *Opt. Exp.*, vol. 17, pp. 22704–22717, 2009.

[11] B. Baumann, E. Götzinger, M. Pircher, and C. K. Hitzenberger, "Single camera based spectral domain polarization sensitive optical coherence tomography," *Opt. Exp.*, vol. 15, pp. 1054–1063, 2007.

[12] C. Fan, Y. Wang, and R. K. Wang, "Spectral domain polarization sensitive optical coherence tomography achieved by single camera detection," *Opt. Exp.*, vol. 15, pp. 7950–7961, 2007.

[13] M. K. Al-Qaisi and T. Akkin, "Polarization-sensitive optical coherence tomography based on polarization-maintaining fibers and frequency multiplexing," *Opt. Exp.*, vol. 16, pp. 13032–13041, 2008.

[14] S. W. Lee, H. W. Jeong, and B. M. Kim, "High-speed spectral domain polarization-sensitive optical coherence tomography using a single camera and an optical switch at 1.3 μm," *J. Biomed. Opt.*, vol. 15, pp. 010501-1–010501-3, 2010.

[15] M. K. Al-Qaisi and T. Akkin, "Swept-source polarization-sensitive optical coherence tomography based on polarization-maintaining fiber," *Opt. Exp.*, vol. 18, pp. 3392–3403, 2010.

[16] M. Pircher, E. Goetzinger, R. Leitgeb, and C. K. Hitzenberger, "Three dimensional polarization sensitive OCT of human skin in vivo," *Opt. Exp.*, vol. 12, pp. 3236–3244, 2004.

[17] T. Schmoll, E. Götzinger, M. Pircher, C. K. Hitzenberger, and R. A. Leitgeb, "Single-camera polarization-sensitive spectral-domain OCT by spatial frequency encoding," *Opt. Lett.*, vol. 35, pp. 241–243, 2010.

[18] H. Wang, M. K. Al-Qaisi, and T. Akkin, "Polarization-maintaining fiber based polarization-sensitive optical coherence tomography in spectral domain," *Opt. Lett.*, vol. 35, pp. 154–156, 2010.

[19] W. C. Kuo, N.-K. C. C. Chou, C. M. Lai, H. J. Huang, S. S. Wang, and J. J. Shyu, "Polarization-sensitive optical coherence tomography for imaging human atherosclerosis," *Appl. Opt.*, vol. 46, pp. 2520–2527, 2007.

[20] K. Wiesauer, M. Pircher, E. Goetzinger, C. K. Hitzenberger, R. Engelke, G. Ahrens, G. Gruetzner, and D. Stifter, "Transversal ultrahigh-resolution polarization sensitive optical coherence tomography for strain mapping in materials," *Opt. Exp.*, vol. 14, pp. 5945–5953, 2006.

[21] M. Pircher, E. Goetzinger, R. Leitgeb, and C. K. Hitzenberger, "Transversal phase resolved polarization sensitive optical coherence tomography," *Phys. Med. Biol.*, vol. 49, pp. 1257–1263, 2004.

[22] III, and N. Kemp, H. Zaatari, J. Park, H. G. Rylander, and T. Milner, "Depth-resolved optic axis orientation in multiple layered anisotropic tissues measured with enhanced polarization-sensitive optical coherence tomography (EPS-OCT)," *Opt. Exp.*, vol. 13, pp. 4507–4518, 2005.

[23] M. Zhao and J. A. Izatt, "Single-camera sequential-scan-based polarization-sensitive SDOCT for retinal imaging," *Opt. Lett.*, vol. 34, pp. 205–207, 2009.

[24] C. Fan and G. Yao, "Single camera spectral domain polarization-sensitive optical coherence tomography using offset B-scan modulation," *Opt. Exp.*, vol. 18, pp. 7281–7287, 2010.